COMMUNICATION

Pyridine-acetaldehyde, a molecular balance to explore the $n \rightarrow \pi^*$ interaction

Received 00th January 20xx,
Accepted 00th January 20xx

DOI: 10.1039/x0xx00000x

Susana Blanco,*[a] Alberto Macario [a] and Juan Carlos López*[a]

The complex pyridine–acetaldehyde is formed through an $n \rightarrow \pi^*$ interaction and a C-H···O contact. The acetaldehyde methyl group internal rotation induces a phase-locked intermolecular oscillation along the Bürgi-Dunitz coordinate. Surprisingly, this sort of molecular balance extracts energy through the $n \rightarrow \pi^*$ interaction to reduce the size of the internal rotation barrier.

Non-covalent interactions determine the structure and properties of molecules, clusters and materials, and are essential forces in all fields of supramolecular chemistry.[1,2] The cooperation of different non-covalent interactions governs protein folding, molecular recognition[3,4] and the structure of biomolecules.[5–8] An individualized study of these interactions in biological systems turn out to be difficult due to the coexistence of such interaction networks and to the perturbations due to the presence of water molecules. In this way, small model systems, such as isolated molecular complexes, have helped to size the common types of non-covalent interactions.[9–12] In addition, diverse types of molecular balances have been designed to explore and quantify these interactions.[13]

An emergent group of non-covalent interactions are those involving a partner with an electron rich region (lone pair or π electrons) and carbonyl fragments or aromatic π systems substituted with electron withdrawing groups via the so called $n \rightarrow \pi^*$[14] or π-hole[15] interactions. $n \rightarrow \pi^*$ interactions observed in carbonyl compounds[16] are structure determinant in small biomolecules[6–8] and proteins.[17,18] The pioneering works of Bürgi and Dunitz[19] set the basis for the understanding of these interactions, related in organic chemistry to the trajectory for the nucleophilic attack to a carbonyl group. Despite its interest, only a few rotational spectroscopy studies have shown these interactions to occur in molecular complexes.[20–22]

Pyridine (PY) or its derivatives can be used as nucleophilic catalysts in acylation reactions.[23] The structures of pre-reactive intermediates of PY with carbonyl compounds are expected to show the signatures of the $n \rightarrow \pi^*$ interactions as recently observed for the PY-formaldehyde (FA) adduct.[22] However, given the weakness of the $n \rightarrow \pi^*$ interaction one wonders if this interaction would still prevail in PY complexes with aldehydes of increasing size, where steric interactions may bring the cluster geometry out of the Bürgi-Dunnitz trajectory (see Figure 1).[19] The structure of the complex PY-acetaldehyde (AC) may give useful information about this question. AC has a CH_3 group that is expected to induce a moderate distortion. On the other hand, the AC methyl group internal rotation, giving rise to tunnelling splittings observable[24] in the rotational spectrum, has a barrier very sensitive to the influence of intermolecular interactions.[25,26] Here we show how the delicate equilibrium between weak attractive and repulsive interactions leads this motion to modulate the $n \rightarrow \pi^*$ interaction coordinate. In this way, the internal rotation of the methyl group acts a sort of molecular balance which explores the $n \rightarrow \pi^*$ interaction energy.

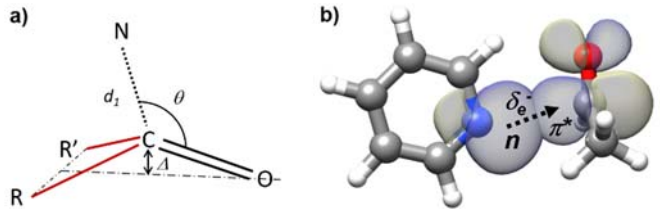

Figure 1 a) Geometrical parameters associated to an $n \rightarrow \pi^*$ interaction between a nucleophile (N) and a carbonyl group. d_1 is the N···C distance ($d1 \leq r_N + r_C$, the sum of van de Waals radii), θ is the ∠N···C=O angle ($\theta = 107 \pm 5º$). For $d_1 < 3.0$ Å the approach path is predicted to lie in the plane bisecting the ∠R'CR angle. Δ reflects the displacement of the C atom from the carbonyl group plane towards the nucleophile. b) Overlap of the *n* donor orbital with the C=O π^* orbital.

The adduct PY-AC was generated (see ESI information for further details) by mixing PY and AC in an Ar or Ne supersonic jet. The rotational spectrum was first recorded using a chirped-pulse microwave Fourier transform spectrometer.[27] Only one

[a] *Departamento de Química Física y Q. Inorgánica. IU CINQUIMA, Facultad de Ciencias, Universidad de Valladolid, E-47011 Valladolid, Spain*

Electronic Supplementary Information (ESI) available: [details of any supplementary information available should be included here]. See DOI: 10.1039/x0xx00000x

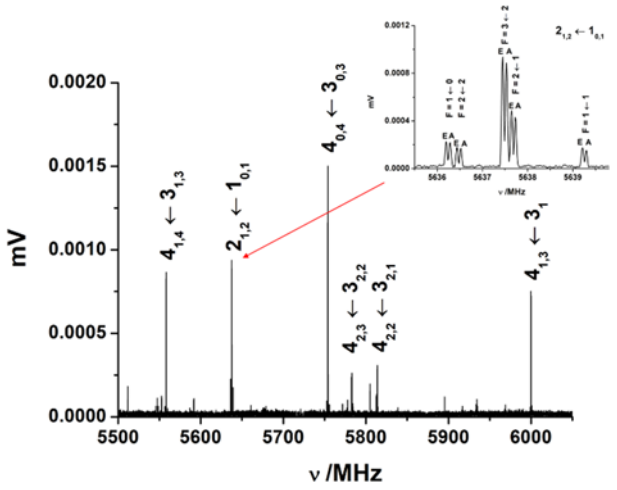

Figure 2. The J=4←3 R-branch μ_a–type spectrum of pyridine-acetaldehyde. The excerpt shows the quadrupole coupling hyperfine structure due to ^{14}N (I=1) and the internal rotation A, E splittings for the μ_b–type $2_{1,2} \leftarrow 1_{0,1}$ transition. The quadrupole coupling components are labelled with the quantum number F (**F= I+J**).

PY-AC species was observed (see Figure 2). Its spectrum shows intense μ_a- and μ_b-type lines, but no μ_c- type lines. The transitions show the quadrupole coupling hyperfine structure due to the presence in PY of ^{14}N nucleus (I = 1). Each transition is further split in two lines due to the coupling of the overall rotation and the AC methyl group internal rotation. Each component of the splitting is labelled as A or E, according to the C_3 symmetry of the methyl torsion states. A summary of the results obtained from the global analysis[28] of the spectrum can be seen in Table 1. The spectra of ^{13}C isotopologues in their natural abundance were also measured in order to investigate the structure of the complex. Complete data sets are given in ESI Tables S1-S3 and S11-S19.

Table 1. A selection of the parameters obtained from the global analysis of the A and E methyl torsion states of the pyridine-acetaldehyde adduct and their comparison with the CCSD/6-311++G(2d,p) ab initio constants for the A1 form (see Figure 3).

Param.[a]	Exp.	Ab	Param.	Exp.	Ab
A/MHz	3633.7214 (8)[b]	3646	V_3/cm^{-1}	343.6(3)	344
B/MHz	778.4311(1)	775	∠*(i,a)*/°	134.4(1)	136.2
C/MHz	667.9241(1)	662	∠*(i,b)*/°	46.2(1)	49.2
χ_{aa}/MHz	-4.016(2)	-4.3	∠*(i,c)*/°	79.80(4)	76.8
χ_{bb}/MHz	0.877(3)	1.0	*n*	373	
χ_{cc}/MHz	3.137(3)	3.4	σ/kHz	3.5	

[a] *A*, *B* and *C* are the rotational constants. χ_{aa}, χ_{bb}, χ_{cc} are the ^{14}N nuclear quadrupole coupling constants. V_3 is the barrier to internal rotation of the methyl group. ∠*(i,α)* (α= *a*, *b* or *c*) are the angles defining the orientation of the methyl top with respect to the principal inertial axes. *n* is the number of hyperfine quadrupole components fitted. σ is the rms deviation of the fit. [b] Standard errors are given in parentheses in units of the last digit.

The comparison of the experimental parameters (Table 1) with those calculated at different theoretical levels[29] (see Tables 1 and S4-S5) for the different forms of the complex shown in Figure 3, allows us to identify the observed PY-AC species as conformer A1. The magnitudes of the calculated electric dipole moment components of A1 are also in good agreement with the observed selection rules. The CCSD/6-311++G(2d,p) is the level which better reproduces the experimental data (see Table S6). The non-observation of other forms (A2-A4) can be attributed

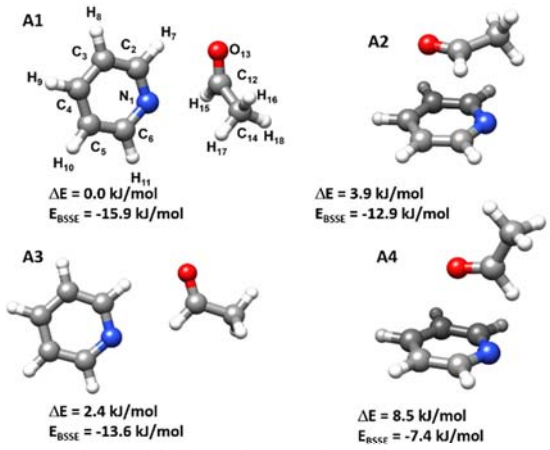

Figure 3. Shapes, labelling, relative and complexation energies of four stable forms of the adduct pyridine-acetaldehyde. Energies are calculated at CCSD(T)/6-311++g(2d,p)//CCSD/6-311++g(2d,p) level. Conformer A1 shows an $n \rightarrow \pi^*$ interaction and a weak C-H···N contact. In A2 the two subunits are stacked. In A3 two weak C-H···N and C-H···O take place. In A4, a C-H···N weak contact is predicted.

to conformational relaxation of these conformers to form A1 in the supersonic jet as was reported for the adduct PY-FA.[22]

The r_s substitution method of Kraitchman[30] is a purely experimental approach that allows us to locate directly the substituted atoms of a molecule or adduct. Multi-isotopic information can also be used to get the effective ground state, r_0, bond distances and angles from a least squares fit of all of the available rotational parameters.[31] The r_s and r_0 results are summarized in Figure 4. The angles measuring the orientation of the methyl top, ∠*(i,a)*, ∠*(i,b)* and ∠*(i,c)*, obtained from the internal rotation analysis (see Table 1) show a total consistency with the values determined from the r_0 or r_s structures. Complete details are given in ESI Tables S6-S9 where they are compared with the *ab initio* structures.

The intermolecular stretching motion between both subunits appears to be almost parallel to the *a* inertial axis of the complex (see figure 4c). The stretching force constant can be then estimated from the experimental value of the D_J centrifugal distortion constant (D_J=1.09899(57) kHz, see Tables S1-S2) within the pseudo diatomic approximation.[32] Its value

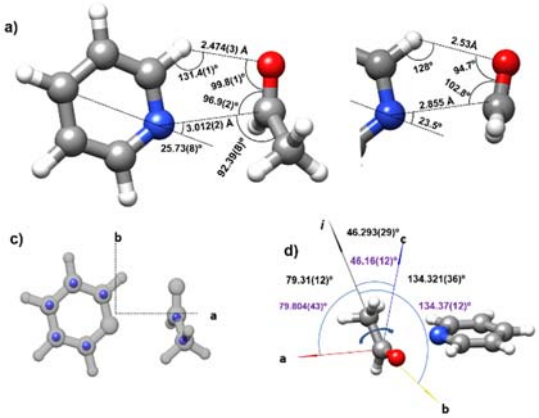

Figure 4. a) The effective r_0 structure of the pyridine-acetaldehyde complex. b) The r_0 data of pyridine-formaldehyde;[22] c) comparison between the r_s and the CCSD/6-311++G(2d,p) r_e structures; d) Definition of the angles ∠*(i,a)*, ∠*(i,b)* and ∠*(i,c)* measuring the orientation of the methyl top with respect to the principal inertial axis and comparison of r_0 (black, up) and internal rotation analysis (purple, down) values.

results to be k_s = 6.166(14) N m^{-1}. Assuming that the intermolecular motion can be described by a Lennard–Jones type potential approximation,[22] the dissociation energy has been estimated[33] to be E_D=9.938(22) kJ/mol, a value lower than those predicted theoretically (see Figure 3).

The experimental structure provides direct evidence of the formation of an $n\rightarrow\pi^*$ interaction. The Bürgi-Dunitz distance, d_1=r(N$_1$···C$_{12}$) = 3.012 Å is shorter than the sum of van der Waals radii, $r_N + r_C$ = 3.25 Å, allowing for orbital overlap.[14] The N atom is deviated *ca.* 14.8° from the axis normal to the acetaldehyde plane consistently with a d_1>3.0 Å value. The Bürgi-Dunitz angle ∠N···C=O is 96.9(2)°, in the limit of the predicted range of 107±10º.[14] So the N atom is not far from the Bürgi-Dunitz[34] trajectory which maximizes n-π* orbital overlap. Moreover, the $n\rightarrow\pi$* interaction coexists with a weak C-H···O hydrogen bond (HB). The geometry of the HB, distance r(H$_7$···O$_{13}$) = 2.474(3) Å and angles ∠C$_{12}$O$_{13}$H$_7$ = 99.8(1)°, ∠C$_2$H$_7$O$_{13}$= 131.4(1)° and ∠C$_{14}$C$_{12}$O$_{13}$H$_7$ = -97.8(2)° indicate, according to general considerations,[35] that this is a very weak contact.

A comparison with the structure of pyridine-formaldehyde (PY-FA), with C_s symmetry, (see Figure 4) reveals that the $n\rightarrow\pi$* interaction is weakened in PY-AC due to the repulsive interactions affecting to the methyl group. This repulsive interaction distort the angle between the pyridine and aldehyde planes from 90° in PY-FA to *ca*. 75.2° in PY-AC. On the other hand the C-H···O weak HB seems to be reinforced in PY-AC if we compare the r(O$_{13}$···H$_7$) distances in both complexes.

The interactions responsible for the formation of A1 form have been further investigated using Quantum Theory of "atoms in molecules" (QTAIM)[36,37] to locate bond paths (BP) and bond critical points (BCP). The results are summarized in Figure 5a where the BPs and BCPs for both the $n\rightarrow\pi$* interaction and the weak C-H···O interactions are shown. Estimation of the interaction energies (see Figure 5a) indicates that both weak interactions have almost the same strength. Comparison of these values with those for the complex PY-FA[22] (see Figure S3) confirms that the $n\rightarrow\pi$* interaction is substantially weakened in PY-AC. In addition, a non-covalent interaction (NCI) analysis[38] has been done in order to visualize the adduct weak interactions. In the NCI plot, intermolecular interactions are visualized as isosurfaces whose colour codes indicate the strengths of attractive or repulsive interactions. The results can be seen in Figure 5b where the greenish isosurface points indicating weak attractive interaction regions can be related to the BCPs (see Figures S2 and S3 for further details).

The formation of the $n\rightarrow\pi$* interaction is usually tested using natural bond orbital (NBO)[12,39] analysis to investigate the donor→acceptor properties characteristic of this interaction (see Figure 1b). The results of this analysis for PY-AC done at RHF/aug-cc-pVTZ level for the CCSD structures are given in Table S10. The stabilization energies, ΔE_{del}, calculated by deletion-type NBO re-optimizations are also given. By far, the strongest intermolecular delocalization occurs from donation of the lone pair (n) of the nitrogen atom to the π* orbital of the carbonyl group (ΔE_{del} = 6.7 kJ/mol). This energy is *ca.* half the value calculated for the complex PY-FA (ΔE_{del} = 12.8 kJ/mol) with a much shorter r(N$_1$···C$_{12}$) distance.[22]

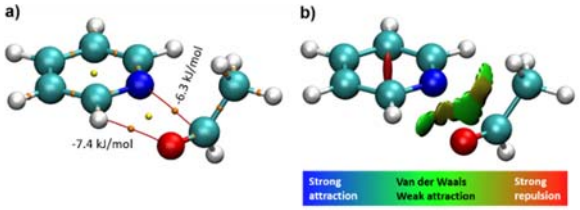

Figure 5. a) Bond paths (BP, red), ring (yellow) and bond (orange) critical points (BCP). The strength of the $n\rightarrow\pi^*$ and C-H···O interactions estimated from the electron potential density $V(r)$ at the BCPs is given. b) Non-covalent interaction (NCI) isosurfaces with S=0.5.

One of the most interesting experimental observations in this work is that the value for the methyl top internal rotation barrier decreases *ca.* 64 cm^{-1} from free AC (V_3=407.59768 cm^{-1})[24] to PY-AC (V_3 = 343.60(32) cm^{-1}). The reason for this change has been investigated by exploring the potential energy along the methyl-top internal rotation coordinate, α (∠H$_{16}$-C$_{14}$-C$_{12}$-O$_{13}$), using *ab initio* methods, in free AC (V_{AC}) and in PY-AC ($V_{PY\text{-}AC}$). Apart from the difference in the V_3 values, the calculations (see Tables S6 and S9b) predict different equilibrium α_e angles for both systems. CCSD method predicts a α_e offset of -4 for PY-AC while MP2 given shorter r(N$_1$···C$_{12}$) distances predict a *ca.* -7° offset. Figure 6 shows the experimental three-fold potential functions of free AC and PY-AC, and the difference between them, $\Delta V(\alpha) = V_{AC} - V_{PY-AC}$, that contains the information to understand the causes of the barrier decrement upon complexation. V_{AC} and $V_{PY\text{-}AC}$ have been represented using the experimental V_3 values but taking into account the -4° CCSD offset in α for PY-AC. Because of this offset, the difference function $\Delta V(\alpha)$ results to have a phase angle τ = 19°.

The structural changes accompanying the methyl group rotation are due to the steric interaction between PY and the AC methyl group that distort the $n\rightarrow\pi$* geometry (see animation in Figure S4). These changes mainly affect to the Bürgi-Dunitz r(N$_1$···C$_{12}$) distance which shows large oscillations as illustrated in Figure 6. Other intermolecular parameters show less pronounced oscillations (see Figure S5). All oscillations turn out to have either the same or opposite phase with respect to the difference function $\Delta V(\alpha)$. The α-dependence of r(N$_1$···C$_{12}$) shown in Figure 6, has exactly an opposite phase relation. Since the energy of the $n\rightarrow\pi^*$ interaction increases for shorter r(N$_1$···C$_{12}$) distances, $\Delta V(\alpha)$ is thus giving a measure of the $n\rightarrow\pi^*$ interaction energy along the range of values of r(N$_1$···C$_{12}$) sampled by the CH$_3$ internal rotation. The NBO stabilization energy, ΔE_{del}, calculated for the range of structures explored by the CH$_3$ internal rotation oscillates with the same phase as that of $\Delta V(\alpha)$ (see Figure S6) but with a higher amplitude.

In summary, we have shown that the structure and properties of the PY-AC complex are the result of the equilibrium between stabilizing interactions and steric repulsive forces. The cooperation of an $n\rightarrow\pi^*$ interaction from the PY nitrogen lone pair to the π^* orbital of the AC carbonyl group and a C-H···O weak HB determine the geometry of the adduct. On the other hand, the repulsive forces between the CH$_3$ group of AC and the PY ring distort the geometry of the $n\rightarrow\pi^*$ interaction. These steric forces affect to the internal rotation of

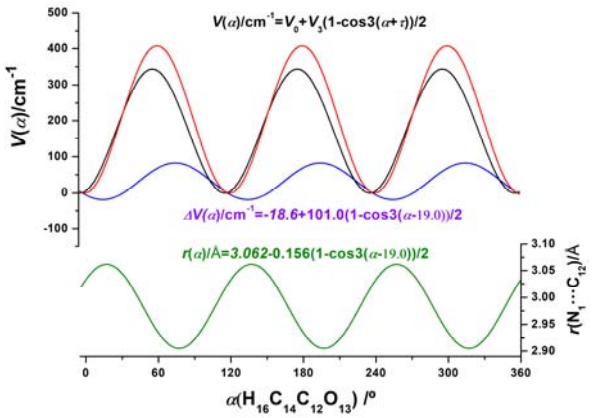

Figure **6**. The methyl top potential energy functions for free acetaldehyde[24] (red, V_0 = 0.0 cm^{-1}, V_3 = 407.6 cm^{-1}, τ = 0º), pyridine-acetaldehyde (black, V_0 = 0.0 cm^{-1}, V_3 = 343.6 cm^{-1}, τ = 4.0º). The difference function $\Delta V(\alpha) = V_{AC}-V_{PY-AC}$ (blue) and the $r(N_1\cdots C_{12})$ distance, which exhibits large oscillations along the minimum energy pathway, have exactly opposite phases.

the CH_3 group in such a way that this motion modulates the $n\rightarrow\pi^*$ geometrical parameters which experience oscillations phase-locked to the internal rotation. This in turn modulates the energy of the $n\rightarrow\pi^*$ interaction which oscillates with a certain amplitude, not far from 100 cm^{-1}, and a constant phase relation with respect to the CH_3 rotation. The net result of this $n\rightarrow\pi^*$ oscillation, independent of any phase relation, is the 64 cm^{-1} experimentally measured reduction of the methyl group internal rotation barrier with respect to its value in free AC. This leads us to conclude that the CH_3 internal rotation is acting as a sort of molecular balance measuring the energy of the $n\rightarrow\pi^*$ interaction for a range of values of the Bürgi-Dunitz coordinate. In other words AC is extracting energy through the PY-AC $n\rightarrow\pi^*$ interaction to reduce the methyl torsion barrier. To our knowledge this is the first time that the energy of the $n\rightarrow\pi^*$ interaction has been explored experimentally in the gas phase.

The authors acknowledge Prof. I. Alkorta (Instituto de Química Médica, CSIC, Madrid, Spain) for his help with theoretical calculations and the Ministerio de Economía y Competitividad (Grant CTQ2016-75253-P) for financial support.

Conflicts of interest

There are no conflicts to declare

Notes and references

1 J. M. Lehn, *Angew. Chemie Int. Ed. English*, 1988, **27**, 89–112.
2 J. M. Lehn, *Science*, 2002, **295**, 2400–2403.
3 A. Dal Corso, M. Catalano, A. Schmid, J. Scheuermann and D. Neri, *Angew. Chemie Int. Ed.*, 2018, **57**, 17178–17182.
4 A. J. Dingley and Stephan Grzesiek, *J. Am. Chem. Soc.*, 1998, **120**, 8293–8297.
5 G. J. Bartlett, R. W. Newberry, B. VanVeller, R. T. Raines and D. N. Woolfson, *J. Am. Chem. Soc.*, 2013, **135**, 18682–18688.
6 S. Blanco, J. C. López, S. Mata and J. L. Alonso, *Angew. Chemie Int. Ed.*, 2010, **49**, 9187–9192.
7 A. Lesarri, E. J. Cocinero, J. C. López and J. L. Alonso, *J. Am. Chem. Soc.*, 2005, **127**, 2572–2579.
8 M. E. Sanz, A. Lesarri, M. I. Peña, V. Vaquero, V. Cortijo, J. C. López and J. L. Alonso, *J. Am. Chem. Soc.*, 2006, **128**, 3812–3817.
9 C. Desfrançois, S. Carles and J. P. Schermann, *Chem. Rev.*, 2000, **100**, 3943–3962.
10 M. T. Doppert, H. van Overeem and T. J. Mooibroek, *Chem. Commun.*, 2018, **54**, 12049–12052.
11 J. Echeverría, *Chem. Commun.*, 2018, **54**, 3061–3064.
12 F. Weinhold and C. R. Landis, *Valency and Bonding*, Cambridge University Press, Cambridge, 2005.
13 I. K. Mati and S. L. Cockroft, *Chem. Soc. Rev.*, 2010, **39**, 4195.
14 R. W. Newberry and R. T. Raines, *Acc. Chem. Res.*, 2017, **50**, 1838–1846.
15 A. Bauzá, T. J. Mooibroek and A. Frontera, *ChemPhysChem*, 2015, **16**, 2496–2517.
16 R. Paulini, K. Müller and F. Diederich, *Angew. Chemie Int. Ed.*, 2005, **44**, 1788–1805.
17 G. J. Bartlett, A. Choudhary, R. T. Raines and D. N. Woolfson, *Nat. Chem. Biol.*, 2010, **6**, 615–620.
18 L. E. Bretscher, C. L. Jenkins, K. M. Taylor, M. L. DeRider and R. T. Raines, *J. Am. Chem. Soc.*, 2001, **123**, 777–778.
19 H. B. Bürgi, J. D. Dunitz, J. M. Lehn and G. Wipff, *Tetrahedron*, 1974, **30**, 1563–1572.
20 Q. Gou, G. Feng, L. Evangelisti and W. Caminati, *Angew. Chem. Int. Ed. Engl.*, 2013, **52**, 11888–11891.
21 C. Pérez, J. L. Neill, M. T. Muckle, D. P. Zaleski, I. Peña, J. C. López, J. L. Alonso and B. H. Pate, *Angew. Chemie Int. Ed.*, 2015, **54**, 979–982.
22 S. Blanco and J. C. López, *J. Phys. Chem. Lett.*, 2018, **9**, 4632–4637.
23 R. Tandon, T. Unzner, T. A. Nigst, N. De Rycke, P. Mayer, B. Wendt, O. R. P. David and H. Zipse, *Chem. A Eur. J.*, 2013, **19**, 6435–6442.
24 I. A. Smirnov, E. A. Alekseev, V. V. Ilyushin, L. Margulés, R. A. Motiyenko and B. J. Drouin, *J. Mol. Spectrosc.*, 2014, **295**, 44–50.
25 J. Thomas, O. Sukhorukov, W. Jäger and Y. Xu, *Angew. Chemie Int. Ed.*, 2014, **53**, 1156–1159.
26 B. Ouyang and B. J. Howard, *Phys. Chem. Chem. Phys.*, 2009, **11**, 366–373.
27 G. G. Brown, B. C. Dian, K. O. Douglass, S. M. Geyer, S. T. Shipman and B. H. Pate, *Rev. Sci. Instrum.*, 2008, **79**, 4–5.
28 H. Hartwig and H. Dreizler, *Z. Naturforsch.*, 1996, **51a**, 923–932.
29 M. J. Frisch et al, *Gaussian Inc., Wallingford, CT,* 2013.
30 J. Kraitchman, *Am. J. Phys.*, 1953, **21**, 17–24.
31 Z. Kisiel, *J. Mol. Spectrosc.*, 2003, **218**, 58–67.
32 D. J. Millen, *Can. J. Chem.*, 1985, **63**, 1477–1479.
33 T. J. Balle, E. J. Campbell, M. R. Keenan and W. H. Flygare, *J. Chem. Phys.*, 1980, **72**, 922–932.
34 H. Burgi, J. Dunitz and E. Shefter, *J. Am. Chem. Soc.*, 1973, **587**, 5065–5067.
35 G. Desiraju and T. Steiner, *The Weak Hydrogen Bond*, Oxford University Press, 2001.
36 R. F. W. Bader, *Chem. Rev.*, 1991, **91**, 893–928.
37 T. Lu and F. Chen, *J. Comput. Chem.*, 2012, **33**, 580–592.
38 E. R. Johnson, S. Keinan, P. Mori-Sánchez, J. Contreras-García, A. J. Cohen and W. Yang, *J. Am. Chem. Soc.*, 2010, **132**, 6498–6506.
39 E. D. Glendening, J. K. Badenhoop, A. E. Reed, J. E. Carpenter, J. A. Bohmann, C. M. Morales and F. Weinhold, *Theor. Chem. Institute, Univ. Wisconsin, Madison*.